High Redshift Galaxy Populations and their Descendants

Qi Guo*, Simon D.M. White
Max Planck Institut für Astrophysik,

arXiv:0809.4259v2 [astro-ph] 26 Sep 2008

ABSTRACT
We study model predictions for the abundance and clustering of high-redshift galaxies, and for the properties of their descendants. We focus on three high-redshift populations: Lyman break galaxies at $z \sim 3$ (LBGs), optically selected star-forming galaxies at $z \sim 2$ (BXs), and distant red galaxies at $z \sim 2$ (DRGs). We select model galaxies from mock catalogues using the observationally defined colour and magnitude criteria. With plausible dust assumptions, our galaxy formation model can simultaneously reproduce the abundances, the redshift distributions and the clustering of all three observed populations. The star formation rates (SFRs) of model LBGs and BXs are lower than those quoted for the real samples, reflecting different initial mass functions and scatter in model dust properties. About 85% of model galaxies selected as DRGs are star-forming, with SFRs ranging up to $\sim 10^2 M_\odot$/yr. Model LBGs, BXs and DRGs together account for less than half of all star formation over the range $1.5 < z < 3.2$; many massive, star-forming galaxies are predicted to be too heavily obscured to appear in these populations. Model BXs have metallicities which agree roughly with observation, but model LBGs are only slightly more metal-poor, in disagreement with recent observational results. The model galaxies are predominantly disk-dominated. Stellar masses for LBGs and BXs are typically $\sim 10^{9.9} M_\odot$, and for DRGs are $\sim 10^{10.7} M_\odot$. Only about 30% of model galaxies with $M > 10^{11} M_\odot$ are classified as LBGs or BXs at the relevant redshifts, while 65% are classified as DRGs. Almost all model LBGs and BXs are the central galaxies of their dark halos, but about a quarter of DRGs are satellites. Half of all LBG descendants at $z = 2$ would be identified as BX's, but very few as DRGs. Clustering increases with decreasing redshift for descendants of all three populations, becoming stronger than that of L^* galaxies by $z = 0$, when many have become satellite galaxies and their mean stellar mass has increased by a factor of 10 for LBGs and BXs, and by a factor of 3 for DRGs. This growth is dominated by star formation until $z \sim 1$ and thereafter by mergers. Merging is predicted to be more important for LBG and DRG descendants than for BX descendants. Most LBGs and DRGs end up as red ellipticals, while BXs have a more varied fate. 99% of local galaxies with $M_* > 10^{11.5} M_\odot$ are predicted to have at least one LBG/BX/DRG progenitor, and over 70% above $10^{11} M_\odot$

Key words: galaxies: star formation – galaxies: colour – galaxies: evolution– cosmology: dark matter – cosmology: large-scale structure

1 INTRODUCTION

The redshift interval $1 < z < 3$ is a very important epoch in the history of galaxy formation. During these several billion years, the star formation rate per unit comoving volume, the abundance of luminous quasars and the specific merger rate of galaxies all reached their peak values. This is when the Hubble sequence of galaxies was established, and most galactic stars were formed.

The last few decades have seen a remarkable development in the observational study of high-redshift galaxies. Using strong the Lyman break feature in the spectrum of star-forming galaxies, Steidel et al. (1996) developed colour-colour criteria to select so-called Lyman Break Galaxies (LBGs) at $z \sim 3$ using deep $U_n GR$ photometry. Extensions of this technique allowed the selection of large samples of star-forming galaxies at lower redshifts, specifically $z \sim 2.3$ (BXs) and $z \sim 1.7$ (BMs) (Adelberger et al. 2004). Recent observations show that there are many high-redshift galaxies with rather little rest-frame UV luminosity which are missed in such optically selected surveys. Franx et al.

* Email: guoqi@mpa-garching.mpg.de

(2003) have successfully developed near-infrared colour criteria to select distant red galaxies (DRGs) at $z \sim 2$ using deep JK photometry. Follow-up observations at a variety of wavelengths have clarified the physical properties of all these high-redshift galaxy populations by providing star-formation rates (Erb et al. 2006a; Reddy et al. 2006), stellar masses (Shapley et al. 2005; Erb et al. 2006b; Kriek et al. 2006; Papovich et al. 2006), morphologies (Abraham et al. 1996; Papovich et al. 2005; Law et al. 2007), dust luminosities (Webb et al. 2003), kinematics (Pettini et al. 2001; Erb et al. 2006b) and clustering estimates (Adelberger et al. 2005; Quadri et al. 2008).

Each of these observational samples provides information on a limited subset of the galaxy population at a specific cosmic epoch, and it is obviously of interest to understand their relation to the population as a whole, both at the redshift of observation and at other redshifts, particularly $z = 0$ where our knowledge of galaxies is best. Within the current standard cosmological paradigm, structure formation in the gravitationally dominant dark matter distribution can be simulated reliably and is now quite well understood (e.g. Springel et al. 2006). For the purposes of modelling galaxy evolution, it can usefully be idealised as a distribution of dark matter halos of "universal" structure which grow steadily in mass through accretion and merging. Galaxies form through condensation of gas within this evolving dark halo population, as first set out by White & Rees (1978). At any given time their distribution can be well modelled by populating halos with galaxies according to a simple recipe, and then adjusting parameters to fit the observed abundance and clustering. The recipe can be based either on a simplified model of the galaxy formation process or on fitting formulae which make no direct reference to the underlying physics (Peacock & Smith 2000; Seljak 2000). The flexibility of the latter Halo Occupation Distribution (HOD) approach allows excellent fits to galaxy luminosity functions and clustering properties at any given epoch (see Cooray & Sheth 2002 for a review) but provides no natural way to link populations at different epochs (see Conroy & Wechsler (2008) for a recent attempt to remedy this). In addition, detailed physical models are needed to assess how observational cuts on luminosity and colour affect the properties of high redshift samples.

A more straightforward approach is to follow galaxy formation directly within the evolving dark matter distribution. This extends the semi-analytic technique developed in the early 1990's (White & Frenk 1991; Kauffmann et al. 1993; Cole et al. 1994), and has made increasingly sophisticated use of information from N-body simulations of cosmic structure formation (Kauffmann et al. 1997, 1999; Springel et al. 2001, 2005). The idea is to design simple parametrised models for the baryonic physics, based either on observation or on more detailed simulations of individual systems, and to implement these recipes in the structure formation framework provided by a dark matter simulation. This provides a powerful tool for studying the formation, evolution and clustering of the galaxy population. It is much less resource-intensive than simulations involving a more direct treatment of baryonic processes, and as a result it allows the treatment of larger volumes and the exploration of a wider range of input parameters and physics recipes. Recent improvements in such modelling have included the move to

higher resolution N-body simulations, enabling use of the substructure information they provide (Springel et al. 2001; Helly et al. 2003; Hatton et al. 2003; Springel et al. 2005; Kang et al. 2005) and the inclusion of additional relevant physics, for example, AGN feedback (Croton et al. 2006; Bower et al. 2006), galactic winds (Bertone et al. 2007) and gas stripping in clusters (Font et al. 2008). These techniques have previously been used to study the properties of LBGs by Blaizot et al. (2004).

The semi-analytic models used in this paper are implemented on the *Millennium Simulation* (Springel et al. 2005, hereafter MS) and are a minor modification of those presented in De Lucia & Blaizot (2007, hereafter DLB07) and Kitzbichler & White (2007, hereafter KW07), which are publicly available at the MS download site[1]. These are refinements of the model originally published as Croton et al. (2006). They have successfully matched a wide range of galaxy properties both locally and at high redshift, but there are some notable discrepancies which demonstrate that the description of galaxy formation physics remains incomplete. Our models (and that of KW07) differ from the model of DLB07 only through the introduction of a redshift dependence in the way dust is treated. We construct light-cone surveys of our models as in KW07, and we select LBGs, BXs, and DRGs exactly as in observational studies. We then compare observed and simulated samples in terms of their abundance, their clustering and their distributions of redshift, colour, metallicity and star formation rate, finding good agreement in most cases. We move on to examine model predictions for the relation of these various populations to each other and to the high-redshift galaxy population as a whole, and for the properties of their descendants at lower redshift.

Our paper is organized as follows. In Sec. 2, we summarize relevant properties of the *Millennium Simulation*, of the semi-analytic model and of our light-cone surveys. Sec. 3 deals with the selection of model LBG, BX and DRG samples, and compares them with observed samples. Sec. 4 examines the relation of these model samples to each other and to the full high-redshift population, and the properties of their descendants. We summarize our results in Sec. 5.

2   GALAXY FORMATION

Our mock galaxy catalogues are constructed by implementing a series of semi-analytic galaxy formation models on stored merger trees which represent the entire growth of nonlinear structure, both dark matter halos and their subhalos, in the very large *Millennium Simulation* (Springel et al. 2005). This simulation assumed a concordance ΛCDM cosmology with parameters consistent with a combined analysis of the 2dFGRS and the first-year WMAP data (Spergel et al. 2003): $\Omega_{\rm m} = 0.25$, $\Omega_{\rm b} = 0.045$, $h = 0.73$, $\Omega_{\Lambda} = 0.75$, $n = 1$, and $\sigma_8 = 0.9$, where the Hubble constant is parameterized as usual as $H_0 = 100h$ km s^{-1}Mpc^{-1}. The *Millennium Simulation* represents the dark matter distribution by following $N = 2160^3$ particles from redshift $z = 127$

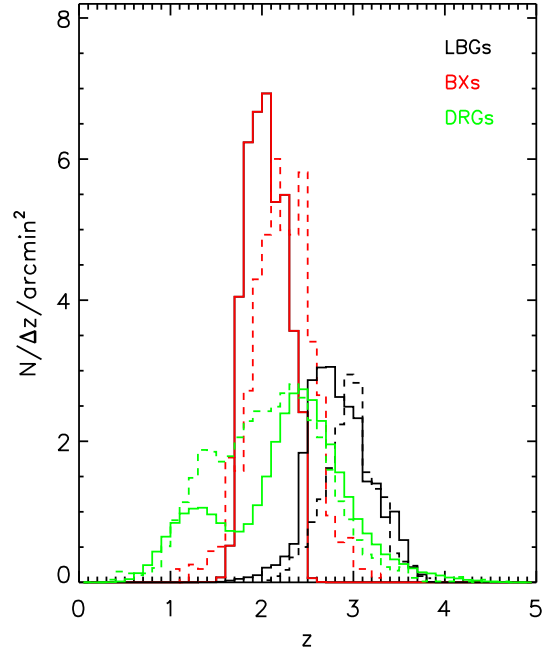[1] http://www.mpa-garching.mpg.de/millennium
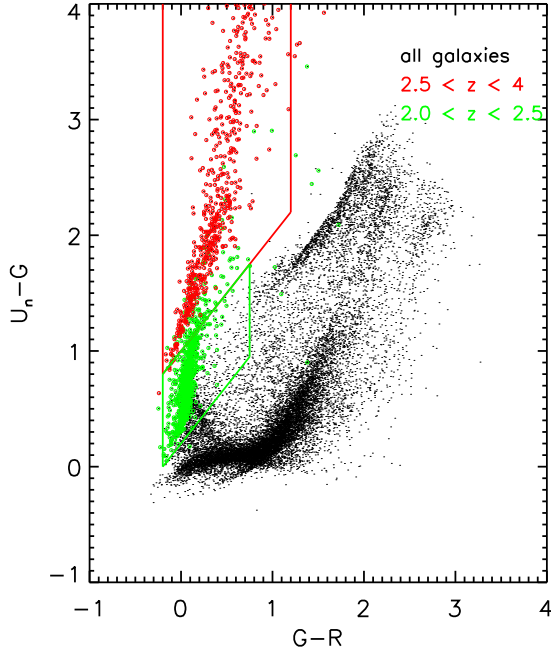
Figure 1. $G - R$ vs. $U_n - G$ diagram for model galaxies selected from a mock redshift survey. The redshift ranges highlighted by coloured circles are indicated in the upper right corner. The red and green boxes outline the original observationally defined selection windows for LBGs and BXs respectively.
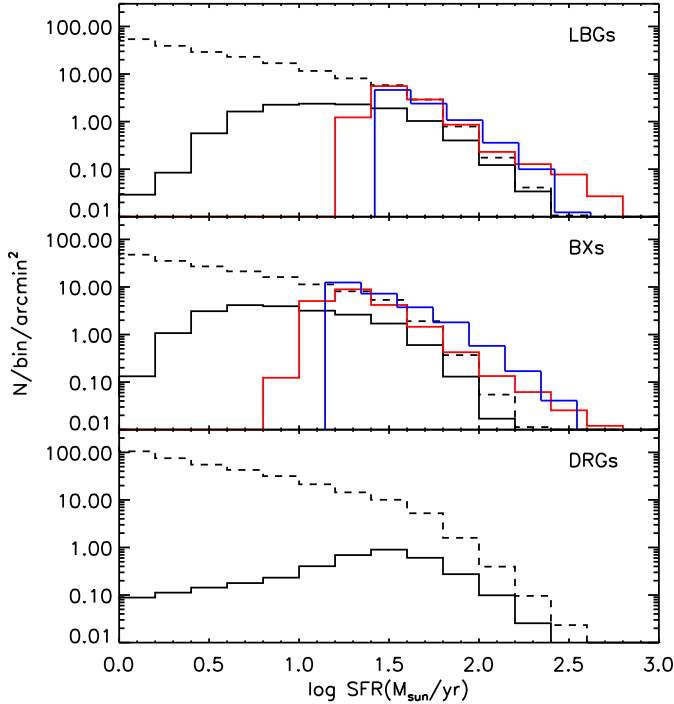

Figure 2. Redshift distributions for LBGs, BXs and DRGs. The solid histograms are for mock galaxies while dashed ones are for the real observed samples. Black histograms indicate LBGs, red ones indicate BXs and green ones indicate DRGs (scaled up in number by a factor of 3 for clarity). Note that the normalisations are given in terms of the surface density of objects on a linear scale, and have not been adjusted. The models do indeed reproduce the observed abundance as a fuction of redshift for all three types of object.

to $z = 0$ in a comoving box of side $500h^{-1}$ Mpc. Each particle thus has a mass of $8.6 \times 10^8 h^{-1} M_\odot$. The simulation data were stored at 64 redshifts apaced approximately logarithmically at early times and linearly at late times. This spacing determines the time resolution of the semi-analytic modelling of galaxy formation, A detailed description of the *Millennium Simulation* can be found in the original article of Springel et al. (2005)

The simulation of the evolution of the galaxy population is based on the modelling techniques developed by the Munich Group. Our galaxy formation model is almost identical to the publicly available model of De Lucia & Blaizot (2007) which is itself a refinement of the model originally implemented on the *Millennium Simulation* by Croton et al. (2006). These models include treatments of gas cooling, star formation and stellar evolution, chemical enrichment, central black hole formation and growth, material and energy feedback both from supernovae and from (radio) AGN, and galaxy merging. The reader is referred to DLB07 and Croton et al. (2006) for detailed descriptions of how these processes are modelled. As was also the case in KW07, we have found it necessary to modify the original treatment of dust attenuation in order to be consistent with high-redshift observations. We describe this in the next section.

2.1 Dust Model

Dust extinction is a crucial ingredient when comparing models of galaxy evolution with observation. In this paper we adopt a simple dust model similar to that used in KW07.

The face-on optical depth is modeled as a function of HI column density and metallicity in the following way:

$$\tau_\lambda^Z = (\frac{A_\lambda}{A_V})_{z_\odot} \eta_Z (\frac{<N_H>}{2.1 \times 10^{21} cm^{-2}}) \tag{1}$$

where A_λ/A_V is the extinction curve estimated in Cardelli et al. (1989) and $< N_H >$ is the the average hydrogen column density. The quantity $\eta_Z = (1 + z)^{-0.4}(Z_{gas}/Z_\odot)^s$ is the redshift- and metallicity-dependent scaling of dust-to-gas ratio, where $s = 1.35$ for $\lambda < 2000A$ and $s = 1.6$ for $\lambda > 2000A$, The metallicity scalings interpolate between the extinction curves measured in the Milky Way and in the two Magellanic Clouds (Guiderdoni & Rocca-Volmerange 1987). The redshift dependence is observationally motivated, based on indictions that dust-to-gas ratios are lower at high redshift than in the local universe for galaxies with the same bolometric luminosity and metallicity (Adelberger & Steidel 2000). In KW07 a similar model was used, except that the redshift dependence was set to be $(1+z)^{-0.5}$ and an artificial disk size evolution with redshift was assumed so that the equivalent redshift dependence of dust extinction became $(1 + z)^{-1}$. There is rather little change in the number count and redshift distribution of galaxies in our mock catalogues when the power index of the redshift dependence is changed from -1 to -0.4. We will show later that the dust model we adopt here pro-

Figure 3. Star formation rate distributions for LBGs, BXs and DRGs. Solid black histograms in each panel refer to model galaxies selected according to the observational colour and magnitude criteria which define the relevant population. They may be compared with the dashed black histograms which give results for all model galaxies in the corresponding redshift range. At all redshifts and SFRs, the observational criteria select fewer than half of all star-forming galaxies. Blue histograms in the LBG and BX panels are direct observational estimates of the SFR distributions for these two populations taken from Reddy et al. (2008). They are clearly centred at higher SFR than in the models. The red histograms show what happens if SFRs are estimated for the model galaxies from their "observed" fluxes assuming the same mean correction for extinction and the same conversion factor from UV luminosity to SFR as in Reddy et al. (2008). The results agree well with the "observed" SFR values but differ substantially from the true values.

duces high-redshift galaxies with the proper number density both at $z \sim 3$ and at $z \sim 2$.

In addition, our dust model assumes that young stars, defined as stars younger than 3×10^7 yr, are more strongly attenuated than the rest of the galaxy. This population is typically still partly embedded in the molecular clouds from which it formed and so is more obscured than the general population. Based on the results of Charlot & Fall (2000), we assume the mean optical depth in front of young stars to be three times that which applies to older populations. In addition, we assign a random inclination to every galaxy and we assume a slab geometry to calculate the effective extinction from the face-on value.

2.2 Light-cone

To make a direct comparison of our galaxy formation simulation with observation, it is necessary to create a deep light-cone survey which mimics a real observational survey.
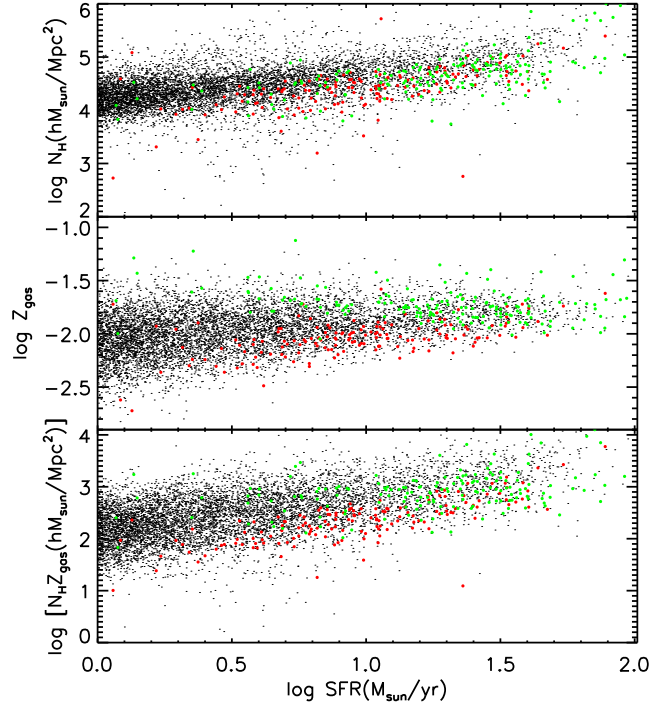
Figure 4. Gas surface density (upper panel), metallicity (middle panel) and the product of the two (bottom panel) plotted against star formation rate for model galaxies at $z = 2.2$. Red and green points are galaxies that satisfy the BX and DRG selection criteria respectively. Black dots correspond to other galaxies, most of which are excluded from either sample because they are too faint.

Here we use techniques developed by KW07 to set up the geometry of the light-cone on the periodic *Millennium Simulation* and to interpolate galaxy properties from the discrete stored outputs to the continuously varying redshift coordinate of the light-cone. The only difference to KW07 is in the dust treatment, as described in the last subsection. We refer the reader to the original paper for detailed descriptions.

For this paper we construct a mock catalogue on an area of 1.4×1.4 square degrees. We calculate apparent magnitudes in the (U_n, G, R) filters used by the KPNO survey of Steidel et al. (2004) and in the (J, H, K) filters used by the MUSYC survey of Quadri et al. (2007a). IGM absorption is modeled by taking into account Lyman series line blanketing, continuum absorption by neutral hydrogen and absorption by heavy elements according to the recipes of Madau (1995). We quote all magnitudes in the AB system. There are a total of 5566388 galaxies in our mock catalogue, of which 393272 and 224604 galaxies are brighter than apparent magnitudes of $R < 25.5$ and $K < 22.86$, respectively. These are the respective limits of the KPNO and MUSYC surveys.

3   MOCK CATALOGUE

3.1   Sample Selection

Owing to the sharp drop-off which it causes at rest-frame 912Å, the Lyman break can be used to identify star-forming galaxies at $z \sim 3$ from optical broad-band photometry.
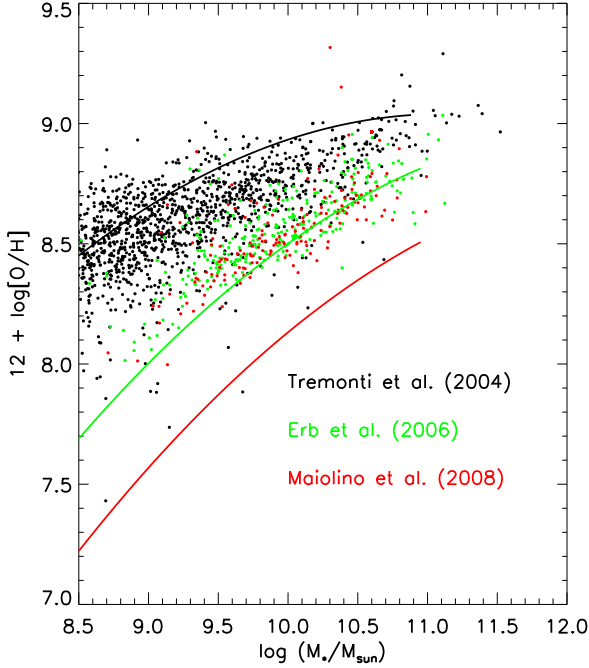
Figure 5. Stellar mass vs. gas-phase metallicity for star-forming galaxies. Black dots represent the low-redshift galaxies, the green dots represent BXs, and the red dots represent LBGs. Observational estimates of the mean relations between these quantities are overplotted using curves with the same colour coding. The sources of the observational relations are indicated by labels

Figure 6. 3D correlation functions for LBGs and BXs. The solid curves are for galaxies from our mock catalogue, while the hatched regions indicate the $\pm 1\sigma$ range for the strength of observed correlations, as quoted by Adelberger et al. (2005). Red curves are for LBGs and black curves are for BXs.

Steidel et al. (1996) developed an effective criterion for identifying such Lyman Break Galaxies (LBGs) based on $U_n - G$ and $G - R$ colours as follows:

$$R \quad \leqslant \quad 25.5 \qquad (2)$$
$$U_n - G \quad \geqslant \quad G - R + 1.0 \qquad (3)$$

A similar technique was later developed by Adelberger et al. (2004) to pick out star-forming galaxies at lower redshifts ($z \sim 2$) so-called BX and BM systems. The criteria proposed for selecting BXs are:

$$R \quad \leqslant \quad 25.5 \qquad (4)$$
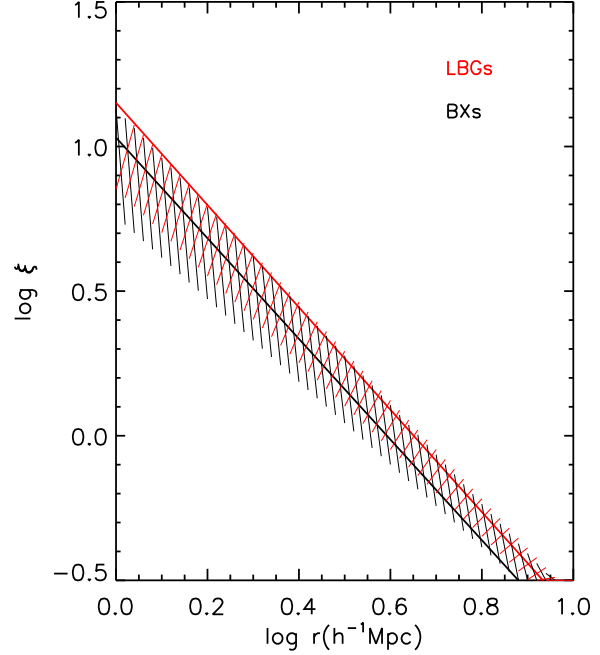$$G - R \quad \geqslant \quad -0.2 \qquad (5)$$
$$U_n - G \quad \geqslant \quad G - R + 0.2 \qquad (6)$$
$$G - R \quad \leqslant \quad 0.2(U_n - G) + 0.4 \qquad (7)$$
$$U_n - G \quad \leqslant \quad G - R + 1.0 \qquad (8)$$

Fig. 1 shows a colour-colour diagram for galaxies in our mock catalogue. Only galaxies with R-band apparent magnitude brighter than 25.5 are shown, in order to mimic the magnitude limit of the observations. Red circles indicate galaxies in the redshift range $2.5 < z < 4.0$, while green circles show galaxies with $2.0 < z < 2.5$. Black dots show galaxies at other redshifts. Red and green boxes outline the colour selection criteria for LBGs and BXs respectively. Clearly our model predicts LBGs and BXs with the proper colours. A careful comparison with Fig.1 in Steidel et al. (2004) shows, however, that the model LBGs and BXs are about 0.2 mag. bluer in $G - R$ colour than the real systems. Our colours

would be shifted to the red by about 0.1 if we adopted a Calzetti dust model (Calzetti et al. 2000) rather than that described above. In our mock catalogues the number densities of LBGs and BXs with $R < 25.5$ are 2.37 and 4.35 per square arcminute, respectively, within 30% of the observational estimates (Steidel et al. 2003, 2004): 1.8 per sq.arcmin for LBGs and 5.2 per sq.arcmin for BXs.

Distant Red Galaxies (DRGs) are K-selected galaxies (Franx et al. 2003) satisfying:

$$K < 22.86 \qquad (9)$$
$$J - K > 1.3 \qquad (10)$$

The number density of such objects in our mock catalogue is 1.16 per sq.arcmin, in good agreement with the observed density of 1.4 per sq.arcmin. More impressively, we also reproduce the number density of a subsample of DRGs with $2 < z < 3$; there are 0.68 per sq.arcmin. in our mock catalogue, in excellent agreement with the observed value of 0.66 per sq.arcmin given by Quadri et al. (2008).

3.2 Redshift Distributions

We show redshift distributions for LBGs, BXs and DRGs in Fig. 2. Black histograms refer to LBGs, red histograms to BXs and green histograms to DRGs. Solid histograms are for model galaxies in our mock catalogue, while the dashed histograms are taken from Steidel et al. (2004) for LBGs and BXs and from Quadri et al. (2008) for DRGs. Note that the normalisations in these histograms have not
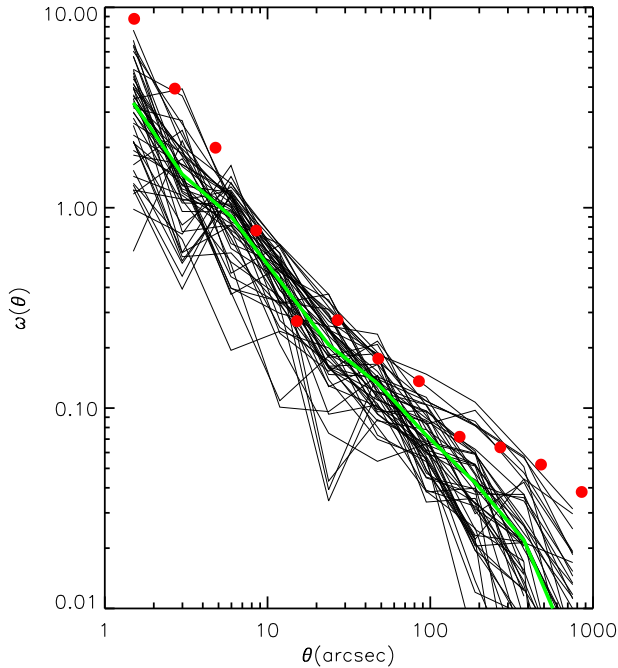
Figure 7. Angular correlation functions for DRGs. Thin black curves are estimates from 48 independent mock catalogues for fields similar in size to that analysed by Quadri et al. (2008). The thick green curve is the average of these 48 model estimates, while the red dots indicate the actual measurement of Quadri et al. (2008).

been adjusted and that the numbers of galaxies are plotted on a linear scale. The redshift distributions for model LBGs and BXs are consistent with observation. although shifted slightly towards lower redshift. Rather than the observed ranges, $2.7 < z < 3.4$ for LBGs and $1.9 < z < 2.7$ for BXs, In our model the LBGs lie primarily in the range $2.5 < z < 3.2$ and the BXs in the range $1.7 < z < 2.5$. These lower redshift BXs correspond to the black dots in Fig. 1 lying within the green selection window. The redshift distribution of DRGs is similar that shown in Quadri et al. (2007a) with a gap between $1.6 < z < 2$. However, recent studies (Quadri et al. 2008; Grazian et al. 2006) show a continous distribution of redshift over $1 < z < 3$. Further observations are needed to reduce photometric redshift uncertainties and to test whether this gap is an artifact or a real feature. Our model suggests that it could be real.

In our mock catalogue, contamination by low redshift interlopers is $\sim 0.9\%$ for LBGs ($z < 2$), $\sim 8\%$ for BXs ($z < 1$) and $\sim 24\%$ for DRGs ($z < 1.8$). These numbers are quite similar to the observational results: $\sim 0.5\%$ for LBGs (Steidel et al. 2003), 6% for BXs (Steidel et al. 2004) and $\sim 15\%$ for DRGs (Reddy et al. 2008). The fraction of galaxies with redshift $2.5 < z < 3.2$ and apparent magnitude $R < 25.5$ which satisfy the LBG colour criteria is 96% in our model. The fraction of galaxies with redshift $1.7 < z < 2.5$ and $R < 25.5$ which satisfy the BX colour criteria is 76%. Both are higher than the observational values quoted by Reddy et al. (2008): 47% for LBGs and 58% for BXs. Photometric errors, which scatter intrinsically more (or less)

luminous galaxies into (or out of) the selection windows may partly account for the low observational completeness. On the other hand, in our model, neither AGN luminosity nor Lyα line luminosity has been taken into account, both of which may affect the selection efficiency.

3.3   Star Formation Rate

We plot the star formation rate distributions of LBGs, BXs and DRGs in Fig. 3. Our model galaxies (solid black histograms) cover a wide range in star formation rate, with average values of $21 M_\odot/\text{yr}$ for LBGs, $11 M_\odot/\text{yr}$ for BXs and $24 M_\odot/\text{yr}$ for DRGs. Observational estimates of star formation rates are shown by the blue histograms (Reddy et al. 2008) and are typically several tens of $M_\odot/\text{yr}$ for LBGs and more than $15 M_\odot/\text{yr}$ for BXs, significantly larger than the values for our model galaxies.

The star formation rate estimates in Fig. 3 were derived from dust-corrected UV magnitudes. Rather than using the actual SFR values for our model galaxies, we can estimate "observational" values from the apparent magnitudes and colours by applying the procedures proposed by Reddy et al. (2008). We derive an "unextincted" UV luminosity for each object by combining its G and R magnitudes to get an approximate rest-frame 1700Å apparent magnitude. We use its redshift to get the corresponding absolute magnitude. We then multiply by 4.5 as a mean correction for extinction. The resulting UV luminosity is converted to a star formation rate using the relation given by Kennicutt (1998) for a Salpeter Initial Mass Function (IMF).

The result is shown in Fig. 3 by the red histograms. These now agree quite well with the "observed" data from Reddy et al. (2008), reflecting the fact that the magnitudes, colours and redshifts of the model galaxies agree quite well with those of the observed populations. The distributions of these "observational" SFR estimates disagree badly, however, with the true SFR distributions in the models. Only a small part of this is due to the fact that the mean extinction in our model is a factor of 3.9, slightly lower than the factor of 4.5 proposed in Reddy et al. (2008). Almost a factor of two comes from the fact that the conversion from UV luminosity to SFR assumes a Salpeter IMF, while the model assumes a Chabrier IMF. The substantial difference in shape reflects the fact that extinction factors vary dramatically from one object to another and are poorly represented by a mean value. Additional dispersion comes from the finite width of the galaxy redshift distribution which affects the conversion from observed magnitudes to rest-frame 1700Å magnitude.

Thus the "observable" properties of our mock samples agree quite well with the real data, but their physical properties suggest that simple SFR estimates based on mean estimates of obscuration can lead to substantial systematic and random errors, in particular to an overestimate of the mean star formation rate.

Comparing the SFR distributions of our photometrically selected samples of model high-redshift galaxies to that for the high-redshift population as a whole (dashed histograms) we find that only around 30% of the galaxies with SFR greater than $5 M_\odot/\text{yr}$ are selected as LBGs or BXs at $z \sim 3$ and $z \sim 2.2$, respectively. We show in Fig. 4 scatter plots of gas mass, gas-phase metallicity and the product of

the two against SFR for all galaxies at $z = 2.2$ separated into those which satisfy the observational BX selection criteria (red) and those that do not (black). We also indicate in green the objects which satisy the DRG selection criteria. BX systems are clearly less obscured than other galaxies with the same SFR. Gas content is the the main contributor to this effect, although metallicity also plays a role. Similar effects are found for model LBGs – there are many objects at the same redshift with similar SFR which are not included in the LBG sample because obscuration makes them too faint. It is interesting to see that in the model there are many DRGs among the highly extincted part of the star-forming galaxy population at $z = 2.2$.

The last panel in Fig. 3 is the SFR distribution of model DRGs. Although selected as red galaxies, most DRGs are, in fact, star-forming. 85% of them fill a rather flat SFR distribution extending from 1 to 40 $M_\odot$/yr and beyond. Only around 15% of the DRGs are passive galaxies with SFR less than 1 $M_\odot$/yr. One thing of interest is to explore the relation between DRGs and BXs. As can be inferred also from Fig. 4, very few DRGs are also BXs. We will discuss this further below.

3.4 Mass-Metallicity Relations

Fig. 5 plots stellar mass against gas-phase metallicity for LBGs (red), for BXs (green) and for $z = 0$ star-forming galaxies (black) in our model. Mean observational relations taken from Tremonti et al. (2004) (for local galaxies),from Erb et al. (2006b) (for BXs) and from Maiolino et al. (2008) (for LBGs) are overplotted as solid curves of the corresponding colour. The mass-metallicity relations for local star-forming galaxies and for BXs are moderately well reproduced by the model. The strong evolution between these two populations reflects the different physical properties of star-forming galaxies at these two well-separated epochs and appears somewhat smaller in the model than in the real data. At early times, the galaxies are more gas-rich and their gas metallicity is relatively low compared to local galaxies of the same stellar mass. The metallicity predicted for BXs is higher than than that for LBGs, but the difference is small, since both BXs and LBGs are selected as UV-bright starforming galaxies and are separated by only 1 Gyr. This is inconsistent with the results of Maiolino et al. (2008); the slope of their observed LBG mass-metallicity relation is consistent with our model, but its normalisation is much lower, indicating a strong apparent evolution between $z \sim 2.2$ and $z \sim 3$. This may reflect calibration uncertainties in the differing metallicity indicators used, rather than true evolution. Further observational study is needed to confirm that evolution is as strong as these datasets indicate.

3.5 Correlation Functions

We show 3D two-point spatial correlation functions for model LBGs (red) and BXs (black) in Fig. 6 and we compare them with observational data from Adelberger et al. (2005). The solid curves are the mean functions for model LBGs and BXs, while the hatched regions between the dashed lines show the $\pm 1\sigma$ range estimated for their observed clustering. For LBGs the model results lie within this one sigma band

but are near its upper limit. For BXs the predicted clustering strength is well centred in the observational band, but the slope of the predicted correlation function is slightly higher than observed.

The number density of DRGs is quite small. To get a more statistically secure result and to estimate how cosmic variance may affect observational clustering measurements, we constructed 48 light-cones for areas of size 0.8×0.8 deg^2. In an attempt to better mimic observational uncertainties, we assign a "photometric redshift" to each model galaxy by adding a random perturbation to its true redshift. Based on the data of Quadri et al. (2008), we set the *rms* value of this perturbation to be $(1 + z) * 0.06 \sim 0.18$. We then study the angular correlation function of DRGs with "photometric" redshifts in the range $2 < z < 3$.The results of this exercise are shown in Fig. 7. The thick green curve represents the mean angular correlation function and the 48 thin curves represent the angular correlation functions estimated in the individual 0.8×0.8 deg^2 regions. The red dots are the observational result of Quadri et al. (2008). At scales between 7 and 100 arcsec, our predictions overlap the observations quite well. At larger and smaller scales, they are low, although one or two of the mock surveys still come close to the observational data.

Quadri et al. (2008) fit line-of-sight projections of simple non-evolving double power-law models to the angular correlation data shown in Fig. 7 and concluded that a comoving correlation length of $10.6 \pm 1.6 h^{-1}$Mpc is needed to match the observations. They noted that in the concordance ΛCDM cosmology, this is significantly larger than expected for *any* galaxy population with the observed abundance of DRG's. We confirm this for own specific model: at $z = 2.24$ objects which satisfy the photometric criteria to be considered DRGs have a comoving correlation length (defined as the scale at which the 3-D spatial correlation function is unity) of $6.6 h^{-1}$Mpc, significantly smaller than the Quadri et al. (2008) value. We have tested whether this apparent discrepancy could be due to the difference in redshift distributions between model and observed DRGs (see Fig. 2). We increase the abundance of DRGs in the redshift range $1.6 < z < 2$. by shifting the $J - K$ colour cut to 1.1 over this interval. This results in a total number density of 1.4 DRGs per sq.arcmin and a continuous redshift distribution over $1 < z < 3$ with no gap. Thus it reproduces the observed distributions well. However, model DRGs with photometric redshifts in $2 < z < 3$ show almost identical angular correlations to our original samples. We conclude that our failure to match precisely the observed redshift distributions has no significant effect on the predicted angular correlations.

It appears that the difference in conclusions here and in Quadri et al. (2008) stems from the fact that we emphasise the agreement of our model with the observed angular correlations over the central part of the measured range, and give less weight to disagreements on the largest and smallest scales, while Quadri et al. (2008) fit the shape of their measured angular correlations quite precisely and then use the correlation length as a measure of clustering strength. At $z = 2.24$, a comoving scale of $10.6 h^{-1}$Mpc corresponds to 540 arcsec, and so is in the range where the observed angular correlations are well above almost all of our mock catalogues. As a result, the DRG correlation length quoted

by Quadri et al. (2008) is larger than that for our model DRGs. Given the noise expected for fields of the observed size (illustrated by the scatter among the thin lines in Fig. 7) it seems likely that a final resolution of this issue will need to wait for a survey of a substantially larger area.

4   THE DESCENDANTS OF HIGH REDSHIFT GALAXIES

In the last section we showed that our galaxy formation simulation reproduces most of the observational properties of the LBGs, BXs and DRGs. The model may therefore provide a useful guide to the physical properties of these systems, as well as to their relations to each other and to lower redshift galaxy populations. We define the descendant of a high-redshift galaxy population, for example the LBGs, to be the set of all galaxies at some lower redshift which have at least one LBG progenitor (which need not be their main progenitor). In the following, we maximise our statistics by selecting high-redshift populations from the full Millennium Simulation volume rather than from a mock catalogue. This can entrain slight differences with the results above because the full data are stored only at discrete epochs and we do not interpolate between them.

4.1   Number Density, Satellite Fraction and Stellar Mass Growth

Table 1 lists predictions from our simulation for the abundance of LBGs, BXs, DRGs and their descendants. The left column is the redshift. The LBG sample is selected as all objects in the MS volume at $z = 3.06$ which would satisfy the observational criteria to be an LBG, if seen on our past light-cone at this redshift. The LBG abundances at lower redshift then refer to the descendants of this population. The BX and DRG populations are similarly selected, but at $z = 2.2$. The abundance of LBG descendants changes very little from $z \sim 3$ to $z \sim 1$, but decreases by 12% by $z = 0$ as a result of mergers. The abundance evolution of BXs and DRGs is similar; there is little change until $z \sim 1$ followed by drops of 10% and 17% to the present day, respectively.

The fractions of model LBGs, BXs, DRGs and their descendants which are satellite galaxies (i.e. are no longer the central galaxy of their dark halo) are shown in Table 2. LBGs and BXs are almost all central galaxies, while 24% of DRGs are already satellite galaxies at the time when they are identified. The satellite fractions among the descendants increase rapidly and become comparable by $z \sim 1$: 45% for LBGs, 39% for BXs and 35% for DRGs. These fractions evolve more slowly at later times. At $z \sim 0$ around half of the descendants are satellite galaxies in all three samples. While DRGs had the largest satellite fraction when they were identified, their descendants actually have the lowest satellite fraction at $z = 0$.

Fig. 8 shows how the descendants of high-redshift galaxies grow in mass.. The solid curves indicate the evolution of the mean stellar mass of each population as a function of redshift. The red, black and green curves are for LBGs, BXs and DRGs, respectively. In all three cases the stellar mass increases relatively slowly until $z \sim 1$ and more rapidly thereafter. This reflects quiet star-formation-dominated growth

Table 1. Comoving number density ($h^3 Mpc^{-3}$) of model LBGs, BXs, DRGs and their descendants

z	LBGs	BXs	DRGs
3	0.00143		
2	0.00142	0.00372	0.00061
1	0.00138	0.00366	0.00058
0	0.00121	0.00332	0.00050

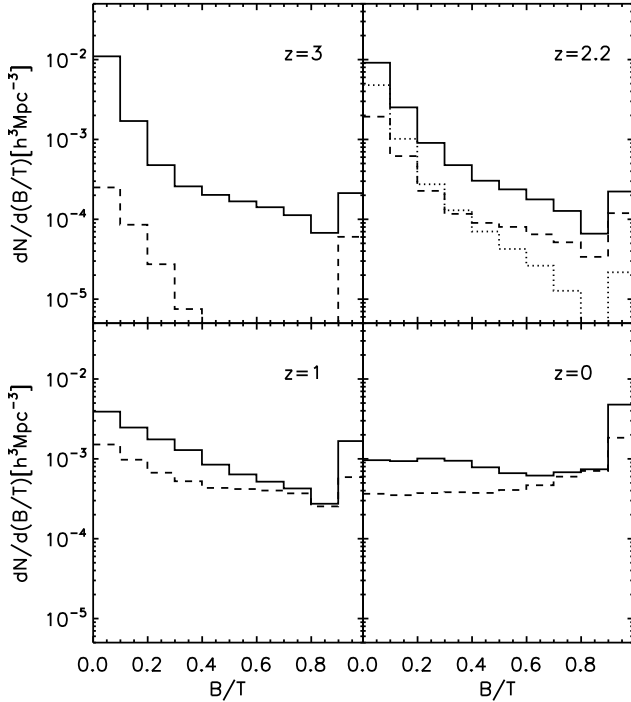**Table 2.** Satellite galaxy fraction among model LBGs, BXs, DRGs and their descendants

z	LBGs	BXs	DRGs
3	0.031		
2	0.235	0.035	0.235
1	0.446	0.386	0.346
0	0.484	0.490	0.386

at early times, followed by merger-dominated growth after $z \sim 1$. To see this more clearly, we also plot as dashed curves the fraction of the mass growth rate at each redshift which is due to star formation, $f_{SF} = \frac{\dot{M}_{SF}}{\dot{M}_*}$. Here $\dot{M}_{SF}$ is the mean star formation rate while $\dot{M}_*$ is the mean of the total stellar mass growth rate. At $z \sim 3$, almost 90% of the stellar mass growth in LBGs is due to star formation. This fraction drops
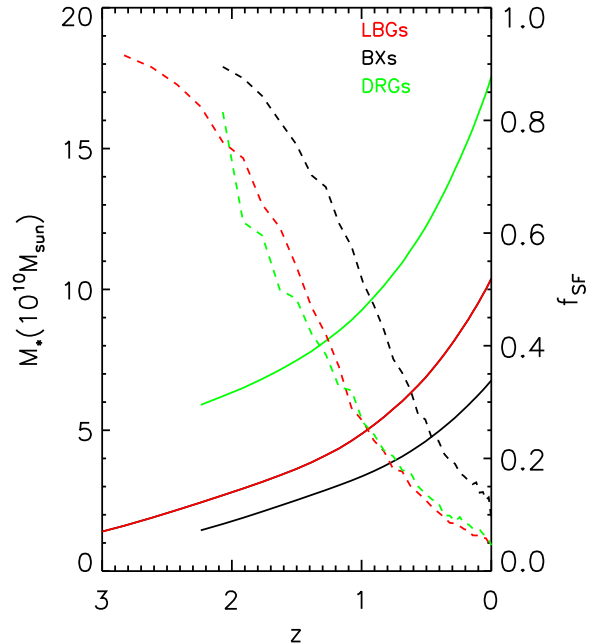
Figure 8. Stellar mass growth in the descendants of high-redshift galaxies. The left axis refers to the mean stellar masses of LBGs, BXs, DRGs and their descendants which are indicated by solid curves. The right axis refers to the fraction of the mass growth rate at each redshift which is due to star formation (the dashed curves). The x-axis is redshift. Red curves are for LBGs, black curves for BXs and green curves for DRGs.

to be spheroids in our model.) This fraction decreases dramatically later on, and more than half of the descendants are bulge-dominated at $z \sim 0$. Indeed, more than a third are ellipticals with B/T greater than 98%. Given the small fraction of the $z \sim 0$ growth rate contributed by star formation (less than 10%) it is clear that the model predicts dry mergers to dominate the recent evolution of LBG descendants. The morphologies of satellite LBGs and satellite LBG-descendants are similar to those of their parent samples, gradually changing from disk-dominated to spheroid-dominated as the population ages.
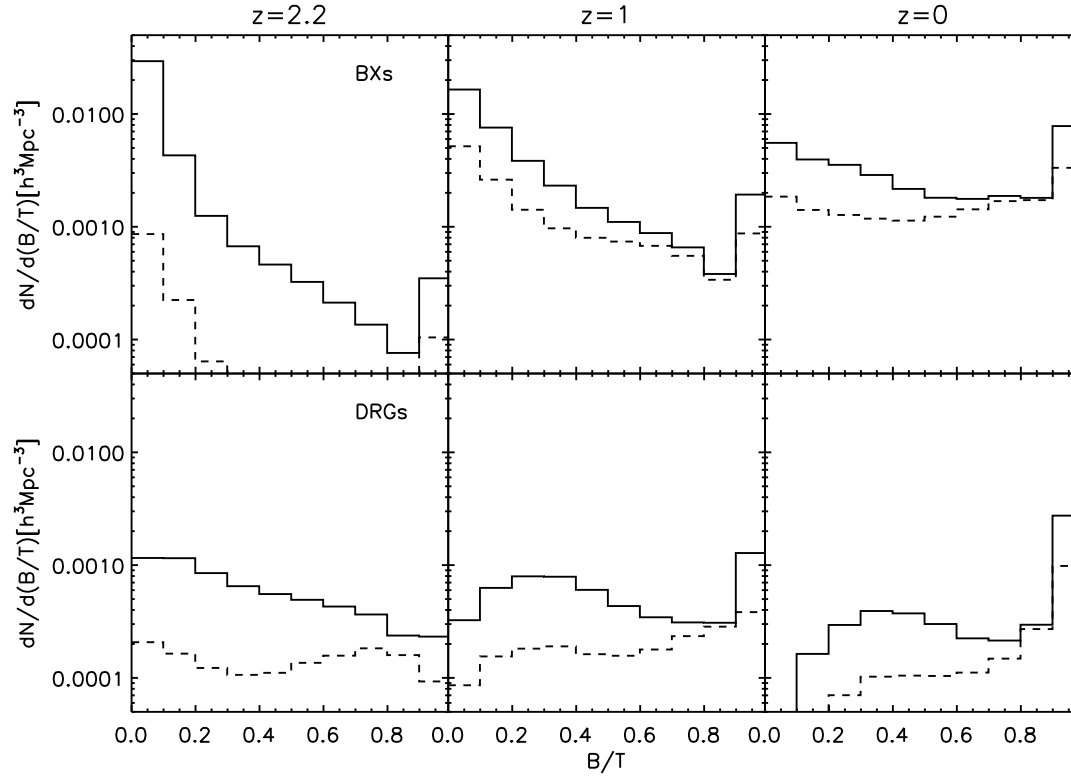
The distributions of bulge-to-total stellar mass ratio for model BXs, DRGs and their descendants are shown in Fig. 10. The BXs behave in a very similar way to the LBGs except that the fraction of disk-dominated systems is larger at all redshifts. Even at $z \sim 0$, around half of all BX descendants are disk-dominated. At the time of identification, most model DRGs are also disk-dominated. By $z \sim 1$ the fraction of pure disk systems among their descendants has dropped by a factor of two. By $z \sim 0$, ellipticals dominate the population of DRG descendants, accounting for 54% of the population; almost no pure disk descendants remain. Mergers clearly play a more important role in the evolution of DRG descendants than in the evolution of LBG and BX descendants.
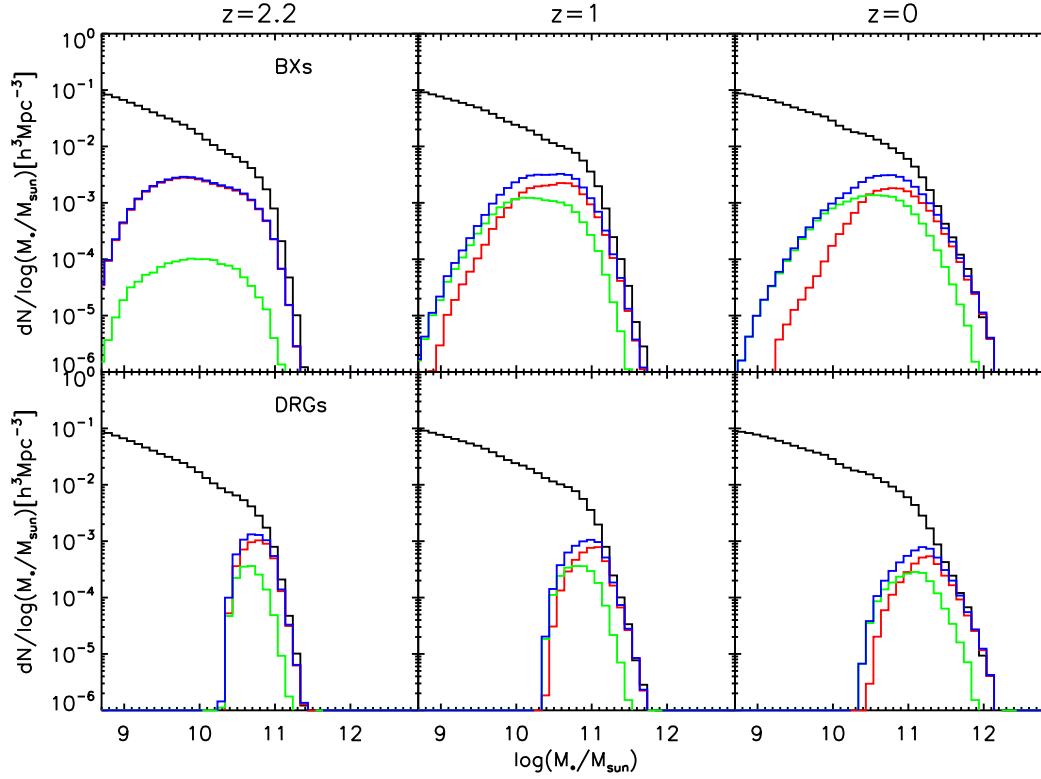
4.3 Stellar Mass Functions

In Fig. 11 we plot stellar mass functions for model LBGs and their descendants and compare these with stellar mass functions for the galaxy population as a whole at each redshift. The LBGs cover a wide range in stellar mass, more than two orders of magnitude, with a peak at $10^{9.9} M_\odot$. As time goes by, the median stellar mass grows by an order of magnitude, becoming more massive than M^* at $z \sim 0$. Very few LBGs end up as central galaxies less massive than $10^{9.9} M_\odot$. Comparing to the overall stellar mass function at $z \sim 0$, we find that 88% of the most massive galaxies ($M_* > 10^{11.5} M_\odot$) are LBG descendants. For $M_* > 10^{11.0} M_\odot$ and $M_* > 10^{10.5} M_\odot$ the corresponding fractions are 34% and 15%, respectively, Thus, most very massive galaxies have at least one LBG as their progenitor. Since fewer than 30% of $z \sim 3$ galaxies with $M_* > 10^{11} M_\odot$ are identified as LBGs, many LBGs were accreted onto more massive non-LBG galaxies during their evolution to low redshift.

The stellar mass functions of satellite galaxy LBGs and central galaxy LBGs are quite similar, but satellite and central galaxies have rather different mass distributions in the descendant populations. The peak of the distribution for satellite galaxies is about a factor of two below that for central galaxies by $z = 0$. Satellite descendants grow less rapidly because almost all mergers occur onto central galaxies and gas cools only onto central galaxies in our model. As a result there are also many more satellites in the low-mass tail of the descendant population.
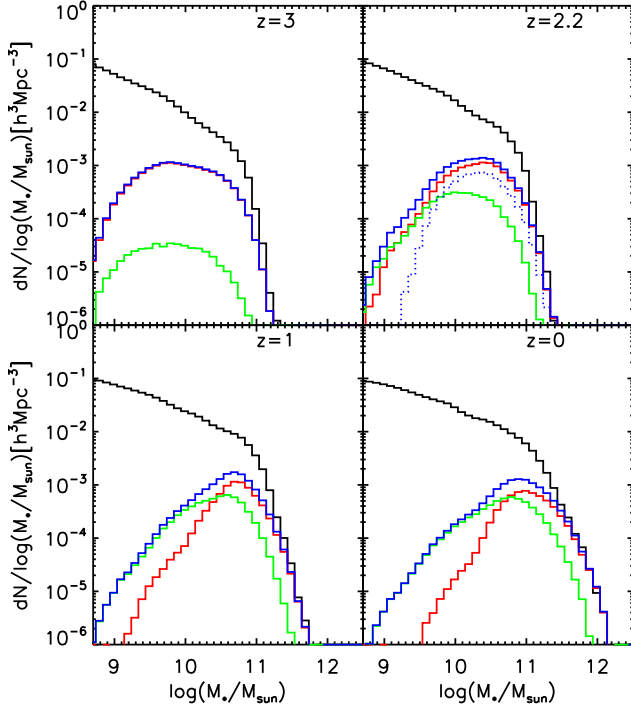
Stellar mass functions for model BXs, DRGs and their descendants are shown in Fig. 12. The results for BXs are again quite similar to those for LBGs and the mass functions peak at the same value. The stellar mass of BX descendants is shifted to slightly lower values than that of LBG descendants and peaks at $10^{10.7} M_\odot$ at $z \sim 0$. At this time 86% of galaxies with $M_* > 10^{11.5} M_\odot$ are BX descendants and

Figure 9. Distributions of bulge-to-total stellar mass ratio for model LBGs and their descendants. The corresponding redshifts are indicated on the upper right corner of each panel. The solid histograms are for all LBGs and their descendants, while dashed histograms show the fraction of each population which are satellite galaxies. The dotted histogram in the upper right panel represents the LBG descendents which would be classified as BXs at $z \sim 2.2$.

with time, and mergers becomes comparable to star formation at $z \sim 1.5$. At the present day, only 5% of the growth in stellar mass of LBG descendants is due to star formation. BXs and their descendants behave in a similar way, star formation accounts for 90% of their stellar mass growth at the time they are identified, but this drops to around 50% by $z \sim 1$ and to only 10% at $z \sim 0$. At any given time, the effect of star formation is more important for BXs than for LBGs. Interestingly, the evolution of f_{SF} for DRGs is always close to that for LBGs. Stellar mass growth is dominated by star formation before $z \sim 1.5$ and by mergers thereafter. The long steady star-formation-dominated epoch between $z \sim 2.3$ and $z \sim 1.5$ reflects the fact that most DRGs in our simulation are highly obscured star-forming galaxies. Note that star formation in this figure includes the starburst mode during mergers. Gas-rich mergers can be an important growth mechanism even before $z \sim 1$.

4.2 Morphology

Fig. 9 shows distributions of bulge-to-total stellar mass ratio (B/T) for model LBGs and their descendants. When identified, most LBGs are disk-dominated (B/T<0.5) systems. The fraction of disk-dominated LBGs remains almost unchanged until $z \sim 2$ and then decreases slowly to $z \sim 1$, showing that gas-rich major mergers are not a dominant mechanism. (The remnants of major mergers are assumed

Figure 10. Distributions of bulge-to-total stellar mass ratio for BXs, DRGs and their descendants. The line-style coding of the histograms is the same as in Fig. 9. The corresponding redshifts are indicated at the top of each column.

Figure 12. Stellar mass functions for model BXs, DRGs and their descendants. The histograms use the same colour coding as in Fig. 11.
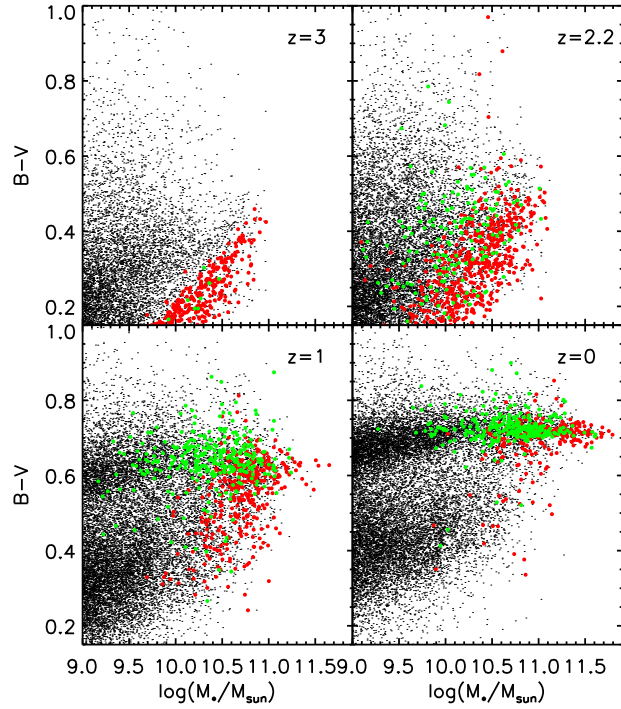
Figure 11. Stellar mass functions for model LBGs and their descendants. Redshifts are indicated in the upper right corner of each panel. Blue histograms are for LBGs and their descendants, red and green histograms split these populations into central and satellite galaxies, respectively. For comparison, stellar mass functions for the galaxy population as a whole are overplotted using black histograms. The dotted blue histogram in the upper right panel shows those LBG descendants which would be identified as BXs at $z \sim 2.2$

Figure 13. B-V colour vs. stellar mass for model LBGs and their descendants at the redshifts indicated in each panel. Red points denote central LBGs and central LBG descendants, while green points denote satellite LBGs and satellite descendants. Black dots indicate other galaxies at the same redshift.

50% of galaxies with $M_* > 10^{11} M_\odot$. For comparison, only 30% of $z \sim 2$ galaxies with $M_* > 10^{11} M_\odot$ are classified as BXs. Unlike the LBGs and BXs, model DRGs span a narrow range of stellar mass at the time they are identified, peaking at $10^{10.7} M_\odot$. By $z \sim 0$ the typical mass of their descendants has increased only by a factor of 3, but almost no descendant is less massive than the Milky Way. DRGs account for more than 65% of galaxies more massive than $10^{11} M_\odot$ at $z \sim 2.2$ and their descendants at $z = 0$ account for more than 84% of galaxies more massive than $10^{11.5} M_\odot$. Many LBGs and BXs are accreted onto massive DRG descendants by $z \sim 0$.

4.4 Colour-Stellar Mass Distributions

In Fig. 13 we show a scatter plot of rest frame $B - V$ colour (AB system) against stellar mass for model LBGs and their descendants, as well as for other galaxies at the corresponding redshifts. When identified, the LBGs are mostly blue galaxies, although none are part of the small red population which already exists at $z \sim 3$. The blue fraction decreases with time. Although their stellar mass has increased by a factor of 2 by $z \sim 2.2$, most of the descendants, especially the central descendants, are blue, indicating a high specific star formation rate. At $z \sim 1$ a significant fraction of the descendants lie on the red sequence. These objects are primarily satellite galaxies where star formation is suppressed.

By $z \sim 0$, most of the descendants, even central descendants, have moved to the red sequence.

Fig. 14 shows similar scatter plots of colour against stellar mass for model BXs, DRGs and their descendants. Yet again the behaviour of the BXs is very similar to that of the LBGs: When selected they are almost all blue galaxies which then gradually move to the red sequence. There are relatively more blue central BX descendants at $z \sim 0$ than blue central LBG descendants. Unlike the LBGs and BXs, most DRGs reside at the massive end of the red sequence in the stellar mass colour diagram, with a typical B-V colour of 0.5. As time goes by, the colour of DRGs gets even redder and they remain on the red sequence. There is almost no difference in colour between their central and satellite descendants.

4.5 The Dark Halos of LBGs

Fig. 15 shows mass distributions for the dark matter halos of model LBGs and their descendants. The dark matter halo here is taken to be the friends-of-friends halo defined by linking together dark matter particles separated by less than 0.2 of the average interparticle separation (Davis et al. 1985). Each FOF halo typically contains several galaxies: one central galaxy and some satellites. Thus, these histograms may count a given halo more than once if it contains several LBGs or LBG descendants. The peak of the halo mass distribution is at $10^{12} M_\odot$ at $z \sim 3$ and moves to $10^{13.4} M_\odot$ by $z \sim 0$, corresponding to the mass of a large galaxy group. At high redshift, central and satellite LBGs live in halos of similar
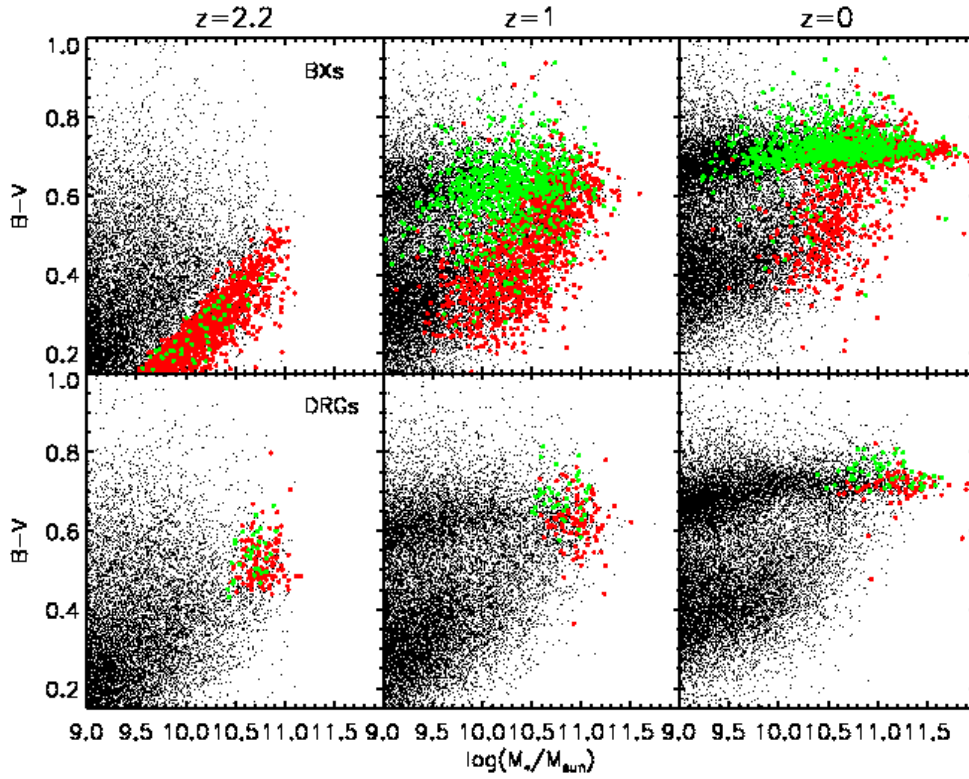
Figure 14. B-V colour vs. stellar mass for model BXs, DRGs and their descendants using the same colour coding as Fig. 13.
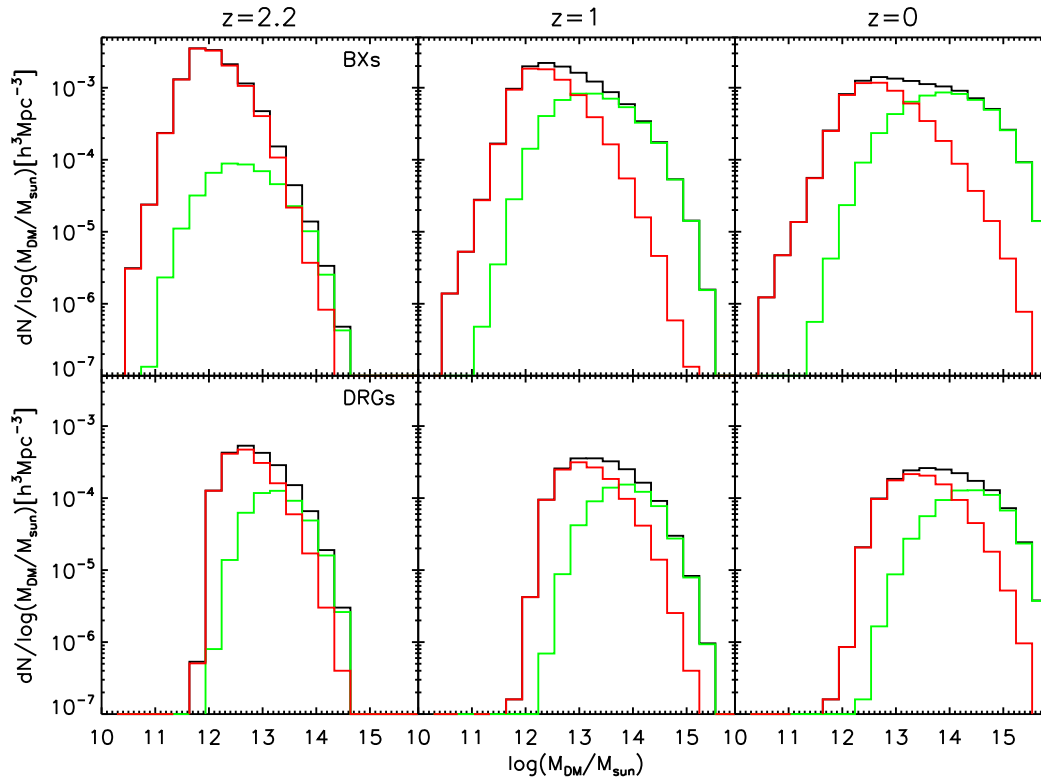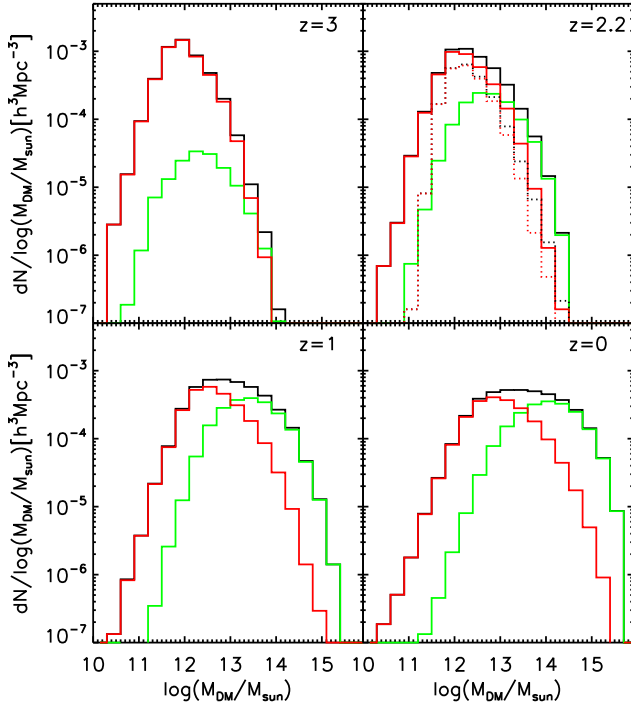

Figure 16. Mass distributions for dark halos of BXs, DRGs and their descendants with the same colour coding as in Fig. 15.

Figure 15. Mass distributions for the dark halos of model LBGs and their descendants. Black histograms are for all objects, while red and green histograms split the sample into central and satellites galaxies, respectively. The dotted black histogram in the upper right panel shows the LBG descendants which would be classified as BXs, while the red dotted histogram shows the subset of these objects which are also central galaxies. Dark halos are multiply counted in these histograms if they contain more than one LBG or LBG descendant.

mass, but at lower redshifts satellite descendants tend to live in more massive halos than central descendants. In fact, the typical present-day environment of central LBG descendants is a poor galaxy group with mass $\sim 10^{13} M_\odot$, while the typical environment of the satellite descendants is a cluster with mass $\sim 10^{14} M_\odot$.

Fig. 16 shows halo mass distributions of model BXs, DRGs and their descendants. As before, BXs are distributed in a similar way to LBGs, although their halos are shifted to noticeably lower masses, peaking at $10^{11.8} M_\odot$ at $z \sim 2$ and then shifting to $10^{12.6} M_\odot$ by $z \sim 0$. For DRGs, the halo masses are larger, peaking at $10^{12.6} M_\odot$ at ~ 2.2 and shifting to $10^{13.4} M_\odot$ by $z \sim 0$. Note that the distribution of halo masses for DRGs is quite narrow compared to that for BXs, consistent with their narrower distribution in stellar mass (Fig. 12). The satellite descendants of BXs and DRGs also more likely be found in more massive halos than their central descendants.

4.6 Descendant Correlations

In a previous section we showed that the correlation functions of our model high-redshift galaxies match observation quite well. Here we look at the evolution of their clustering. In Fig. 17, we plot 3D correlation functions as a function of redshift. For all three populations, the clustering of descen-
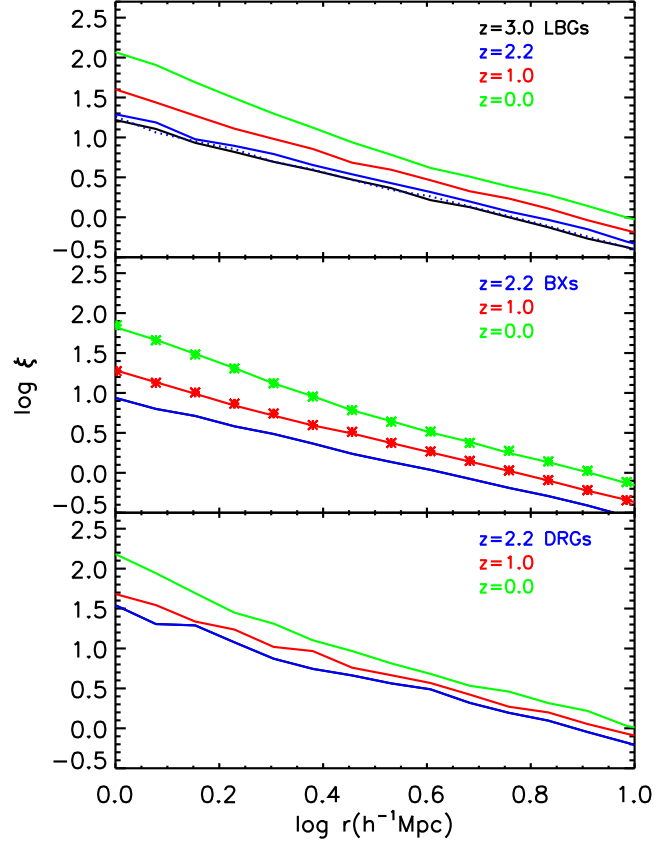
Figure 17. 3D correlation functions for LBGs, BXs, DRGs and for their descendants. Redshifts are indicated at the right upper corner of each panel using the appropriate colour. Solid curves represent the results for full samples of LBGs, BXs, DRGs or their descendants. The dotted curve in the upper panel represents the correlation for LBG descendants which are BXs at $z \sim 2.2$. Stars in the middle panel show correlations at later times of the dark matter particles identified as BXs at $z \sim 2.2$ and so represent how correlations would evolve in a non-merger scenario.

dants gets stronger towards lower redshift. For LBG descendants, the correlation length is $9.7h^{-1}$Mpc at $z = 0$, as estimated from a power law fit over $3h^{-1}$Mpc$< r < 10h^{-1}$Mpc. This is about twice the comoving value at $z \sim 3$. The difference between $z \sim 3$ and $z \sim 2.2$ is quite small compared to changes at later times. At low redshifts there is an obvious turn-up in clustering strength at small scales, indicating the increasing importance of satellite galaxies which we already noted above.

The clustering of BX descendants increases similarly with time, but is always weaker than that of LBG descendants. Their correlation length reaches $8.1h^{-1}$Mpc at $z = 0$. The turn-up at small scales also shows up for BX descendants at low redshift. The comoving correlation length of DRGs evolves less than that of LBGs and BXs, reaching $10h^{-1}$Mpc at $z = 0$. Indeed the correlations of DRG descendants and LBG descendants are almost identical at $z = 0$. For all three populations, the present-day correlation lengths are larger than for L^* galaxies, as might be expected given that their typical stellar masses are higher than M^*.

It is interesting to check whether galaxy merging has

any significant effect on these descendant correlations. We have tested this by by tagging the dark matter particles associated with each BX galaxy at the time it is identified, and then calculating correlations for this particle set at later redshifts. The results are indicated by stars in the central panel of Fig. 17. Clearly, this procedure produces results which are indistinguishable from those obtained by following BX descendants through the *Millennium Simulation* galaxy trees. This validates one part of the simplified recipe adopted by Conroy & Wechsler (2008) and Quadri et al. (2007) when estimating clustering for the descendants of high redshift galaxy populations based on simple HOD assignments of the high-redshift objects to dark halos. Valid results from such recipes will still, of course, require that they assign galaxies to the correct high-redshift halos.

4.7 Relation between LBGs, BXs and DRGs

At $z \sim 2.2$, only 0.8% of model BXs and 10% of LBG descendants are classified as DRGs. Conversely, 4.7% and 25% of DRGs are identified as BXs and LBG descendants, respectively. The overlap between DRGs and BXs or LBG descendants is thus quite small.

In contrast, LBGs and BXs are closely correlated. Fully 45% of LBG descendants at $z \sim 2.2$ are identified as BXs. We illustrate the properties of these particular LBG descendants (which we refer to as LBG-BXs in the following) in the right upper panels of Fig. 9, Fig. 11 and Fig. 15 using dotted histograms. Their distribution in stellar mass is similar to that of all LBG descendants, but with fewer galaxies in the low-mass tail, which consists of satellite galaxies and small central galaxies. Very few satellite galaxies have enough star formation to qualify as BXs in our model, and only 5% of LBG-BXs are satellites, as compared to 23.5% of all LBG descendants. Some of the more massive LBG descendants fail to be identified as BXs because they are rich in gas and heavy elements, and the associated extinction pushes them outside the BX detection window, even though they are strongly star-forming. LBG-BXs are more massive than the overall BX population at $z \sim 2.2$, and this is reflected in their stronger clustering, as shown in the upper panel of Fig. 17. Their clustering is similar to that of LBG descendants in general. A related coincidence shows up in the halo mass distributions which are very similar for the two populations (Fig.15). Since mergers play a minor role in the evolution of LBG descendants before $z \sim 2.2$, the LBG-BXs are, as expected, mainly disk-dominated.

5   SUMMARY AND DISCUSSION

We have used the De Lucia & Blaizot (2007) model for galaxy formation within the *Millennium Simulation* to explore the likely physical nature of observed high-redshift galaxies, specifically Lyman Break Galaxies, BX galaxies and Distant Red Galaxies, and their likely descendants at lower redshift. We first built mock catalogues in order to compare observed high-redshift galaxies with similarly selected objects in the simulation. We then used the full galaxy catalogue from the simulation to study the descendants of the high-redshift populations. We found it necessary to modify the original DLB07 dust model in order to match the

abundance and colour of the observed high-redshift populations,

Impressively, with a proper dust model it is possible to match the observed abundances, redshift distributions and clustering of all three high-redshift populations in a model which also fits the properties of low-redshift galaxies. The descendants of all three populations become more strongly clustered at lower redshifts, and all are more clustered than M^* galaxies today. A turn-up in clustering strength at small scales is evident at $z \sim 0$, which reflects the high satellite fraction among the descendents. The clustering of DRGs is the least consistent with observation. Angular correlations are well reproduced on scales between 7 and 100 arcsec but our model appears more weakly clustered than real DRGs on both smaller and larger scales. This results in an estimated correlation length for the observed sample which is larger than that of our model DRGs. Our results show the expected scatter in angular correlation estimates to be quite large for areas as small as that currently observed, so a final judgement on this issue will require significantly larger observational surveys.

Together, model DRGs and BXs account for only 30% of the strongly star-forming galaxies ($\dot{M}_* > 20 M_\odot / yr$) at $z \sim 2$. Most of the rest are gas- and metal-rich systems which are strongly obscured. In contrast, the model suggests that only 15% of all galaxies with $M_* > 10^{11} M_\odot$ at $z \sim 2$ (most of which do indeed have high star formation rates) are missing in current optical and near-infrared surveys. Interestingly, the model predicts most DRGs to be star-forming galaxies. Their average SFR is even higher than those of LBGs and BXs, and they account for more than 65% of the galaxies with $M_* > 10^{11} M_\odot$ at $z \sim 2.2$. There is rather little overlap between these star-forming DRGs and BXs or LBG descendants. On the other hand, half of all LBG descendants are identified as BXs at $z \sim 2.2$. The physical properties and the clustering of these LBG-BXs are quite similar to those of other LBG descendants. These consist of three classes of galaxy: smaller galaxies where the potential is too shallow to retain the gas expelled by supernova feedback, satellite galaxies where the interstellar gas has been exhausted, and gas-rich galaxies where the dust extinction is strong.

Our simulation roughly reproduces the observed relation between stellar mass and gas-phase metallicity for local star-forming galaxies and for BX galaxies, but the gas-phase metallicities predicted for LBGs, although slightly lower than for BXs, are well above the values estimated for real LBGs by Maiolino et al. (2008).

Most model LBGs, BXs and DRGs are disk-dominated systems, residing at the centres of their own halos. LBGs and BXs are selected as blue galaxies and so exclude the significant population of red galaxies which is already present at these redshifts. Nevertheless, by $z \sim 0$ at least half of their descendants are bulge-dominated and red. The typical stellar masses of LBGs and BXs increase by an order of magnitude by $z \sim 0$, whereas DRG stellar masses increase by a smaller factor, ~ 3. Star formation is the main driver of growth before $z \sim 1$, then mergers become dominant. Most low-redshift massive galaxies ($M_* > 10^{11} M_\odot$) descend from at least one of these high redshift populations. Correspondingly, most descendants are massive galaxies living in massive dark matter halos today. Many of them are satellite galaxies in galaxy clusters. The central galaxies in

rich clusters ($M > 10^{14.7}M_\odot$) typically have 8.4 LBG, BX or DRG progenitors, and on average the stars present in the high-redshift galaxies account for around 50% of the current stellar mass. Thus while the observed high-redshift galaxies have contributed significantly to today's massive galaxies, it appears that the relation between the two populations is quite complex.

ACKNOWLEDGMENTS

REFERENCES

Abraham R. G., van den Bergh S., Glazebrook K., Ellis R. S., Santiago B. X., Surma P., Griffiths R. E., 1996, ApJS, 107, 1

Adelberger K. L., Steidel C. C., 2000, ApJ, 544, 218

Adelberger K. L., Steidel C. C., Pettini M., Shapley A. E., Reddy N. A., Erb D. K., 2005, ApJ, 619, 697

Adelberger K. L., Steidel C. C., Shapley A. E., Hunt M. P., Erb D. K., Reddy N. A., Pettini M., 2004, ApJ, 607, 226

Bertone S., De Lucia G., Thomas P. A., 2007, MNRAS, 379, 1143

Blaizot J., Guiderdoni B., Devriendt J. E. G., Bouchet F. R., Hatton S. J., Stoehr F., 2004, MNRAS, 352, 571

Bower R. G., Benson A. J., Malbon R., Helly J. C., Frenk C. S., Baugh C. M., Cole S., Lacey C. G., 2006, MNRAS, 370, 645

Calzetti D., Armus L., Bohlin R. C., Kinney A. L., Koornneef J., Storchi-Bergmann T., 2000, ApJ, 533, 682

Cardelli J. A., Clayton G. C., Mathis J. S., 1989, ApJ, 345, 245

Charlot S., Fall S. M., 2000, ApJ, 539, 718

Cole S., Aragon-Salamanca A., Frenk C. S., Navarro J. F., Zepf S. E., 1994, MNRAS, 271, 781

Conroy C., Shapley A. E., Tinker J. L., Santos M. R., Lemson G., 2007, ArXiv e-prints, 711

Conroy C., Wechsler R. H., 2008, ArXiv e-prints, 805

Croton D. J., Springel V., White S. D. M., De Lucia G., Frenk C. S., Gao L., Jenkins A., Kauffmann G., Navarro J. F., Yoshida N., 2006, MNRAS, 365, 11

Davis M., Efstathiou G., Frenk C. S., White S. D. M., 1985, ApJ, 292, 371

De Lucia G., Blaizot J., 2007, MNRAS, 375, 2

Erb D. K., Steidel C. C., Shapley A. E., Pettini M., Reddy N. A., Adelberger K. L., 2006a, ApJ, 647, 128

Erb D. K., Steidel C. C., Shapley A. E., Pettini M., Reddy N. A., Adelberger K. L., 2006b, ApJ, 646, 107

Font A. S., Bower R. G., McCarthy I. G., Benson A. J., Frenk C. S., Helly J. C., Lacey C. G., Baugh C. M., Cole S., 2008, MNRAS, pp 1000–+

Franx M., Labbé I., Rudnick G., van Dokkum P. G., Daddi E., Förster Schreiber N. M., Moorwood A., Rix H.-W.,

Röttgering H., van de Wel A., van der Werf P., van Starkenburg L., 2003, ApJ, 587, L79

Grazian A., Fontana A., Moscardini L., Salimbeni S., Menci N., Giallongo E., de Santis C., Gallozzi S., Nonino M., Cristiani S., Vanzella E., 2006, A&A, 453, 507

Guiderdoni B., Rocca-Volmerange B., 1987, A&A, 186, 1

Hatton S., Devriendt J. E. G., Ninin S., Bouchet F. R., Guiderdoni B., Vibert D., 2003, MNRAS, 343, 75

Helly J. C., Cole S., Frenk C. S., Baugh C. M., Benson A., Lacey C., 2003, MNRAS, 338, 903

Kang X., Jing Y. P., Mo H. J., Börner G., 2005, ApJ, 631, 21

Kauffmann G., Colberg J. M., Diaferio A., White S. D. M., 1999, MNRAS, 303, 188

Kauffmann G., Nusser A., Steinmetz M., 1997, MNRAS, 286, 795

Kauffmann G., White S. D. M., Guiderdoni B., 1993, MNRAS, 264, 201

Kennicutt Jr. R. C., 1998, ARA&A, 36, 189

Kitzbichler M. G., White S. D. M., 2007, MNRAS, 376, 2

Kriek M., van Dokkum P. G., Franx M., Förster Schreiber N. M., Gawiser E., Illingworth G. D., Labbé I., Marchesini D., Quadri R., Rix H.-W., Rudnick G., Toft S., van der Werf P., Wuyts S., 2006, ApJ, 645, 44

Law D. R., Steidel C. C., Erb D. K., Pettini M., Reddy N. A., Shapley A. E., Adelberger K. L., Simenc D. J., 2007, ApJ, 656, 1

Madau P., 1995, ApJ, 441, 18

Maiolino R.,Nagao T., Grazian A., Cocchia F.,Marconi A., Mannucci F., Cimatti A., Pipino A.,Ballero S., Calura F., Chiappini C., Fontana A., Granato G. L., Matteucci F., Pastorini G.,Pentericci L., Risaliti G., Salvati M., Silva L., 2008, ArXiv e-prints, 2008, ArXiv e-prints, 806

Papovich C., Dickinson M., Giavalisco M., Conselice C. J., Ferguson H. C., 2005, ApJ, 631, 101

Papovich C., Moustakas L. A., Dickinson M., Le Floc'h E., Rieke G. H., Daddi E., Alexander D. M., Bauer F., Brandt W. N., Dahlen T., Egami E., Eisenhardt P., Elbaz D., Ferguson H. C.,Giavalisco M., Lucas R. A., Mobasher B., Pérez-González P. G., Stutz A., Rieke M. J., Yan H., 2006, ApJ, 640, 92

Peacock J. A., Smith R. E., 2000, MNRAS, 318, 1144

Pettini M., Shapley A. E., Steidel C. C., Cuby J.-G., Dickinson M., Moorwood A. F. M., Adelberger K. L., Giavalisco M., 2001, ApJ, 554, 981

Quadri R., Marchesini D., van Dokkum P., Gawiser E., Franx M., Lira P., Rudnick G., Urry C. M., Maza J., Kriek M., Barrientos L. F., Blanc G. A., Castander F. J., Christlein D., Coppi P. S., Hall P. B., Herrera D., Infante L., Taylor E. N., Treister E., Willis J. P., 2007a, AJ, 134, 1103

Quadri R., van Dokkum P., Gawiser E., Franx M., Marchesini D., Lira P., Rudnick G., Herrera D., Maza J., Kriek M., Labbé I., Francke H., 2007, ApJ, 654, 138

Quadri R. F., Williams R. J., Lee K.-S., Franx M., van Dokkum P., Brammer G. B., 2008, ArXiv e-prints, 808

Reddy N. A., Steidel C. C., Fadda D., Yan L., Pettini M., Shapley A. E., Erb D. K., Adelberger K. L., 2006, ApJ, 644, 792

Reddy N. A., Steidel C. C., Pettini M., Adelberger K. L., Shapley A. E., Erb D. K., Dickinson M., 2008, ApJS, 175, 48

Seljak U., 2000, MNRAS, 318, 203

Shapley A. E., Steidel C. C., Erb D. K., Reddy N. A., Adelberger K. L., Pettini M., Barmby P., Huang J., 2005, ApJ, 626, 698

Spergel D. N., Verde L., Peiris H. V., Komatsu E., Nolta M. R., Bennett C. L., Halpern M., Hinshaw G., Jarosik N., Kogut A., Limon M., Meyer S. S., Page L., Tucker G. S., Weiland J. L., Wollack E., Wright E. L., 2003, ApJS, 148, 175

Springel V., Frenk C. S., White S. D. M., 2006, Nature, 440, 1137

Springel V., White S. D. M., Jenkins A., Frenk C. S., Yoshida N., Gao L., Navarro J., Thacker R., Croton D., Helly J., Peacock J. A., Cole S., Thomas P., Couchman H., Evrard A., Colberg J., Pearce F., 2005, Nature, 435, 629

Springel V., White S. D. M., Tormen G., Kauffmann G., 2001, MNRAS, 328, 726

Steidel C. C., Adelberger K. L., Shapley A. E., Pettini M., Dickinson M., Giavalisco M., 2003, ApJ, 592, 728

Steidel C. C., Giavalisco M., Pettini M., Dickinson M., Adelberger K. L., 1996, ApJ, 462, L17+

Steidel C. C., Shapley A. E., Pettini M., Adelberger K. L., Erb D. K., Reddy N. A., Hunt M. P., 2004, ApJ, 604, 534

Tremonti C. A., Heckman T. M., Kauffmann G., Brinchmann J., Charlot S., White S. D. M., Seibert M., Peng E. W., Schlegel D. J., Uomoto A., Fukugita M., Brinkmann J., 2004, ApJ, 613, 898

Webb T. M., Eales S., Foucaud S., Lilly S. J., McCracken H., Adelberger K., Steidel C., Shapley A., Clements D. L., Dunne L., Le Fèvre O., Brodwin M., Gear W., 2003, ApJ, 582, 6

White S. D. M., Frenk C. S., 1991, ApJ, 379, 52

White S. D. M., Rees M. J., 1978, MNRAS, 183, 341